Sensors & Actuators: B. Chemical 344 (2021) 130154

Contents lists available at ScienceDirect

Sensors and Actuators: B. Chemical

journal homepage: www.elsevier.com/locate/snb

Optical fibre sensor for simultaneous temperature and relative humidity measurement: Towards absolute humidity evaluation

Chenyang He, Serhiy Korposh, Ricardo Correia, Liangliang Liu, Barrie R. Hayes-Gill, Stephen P. Morgan *

Optics and Photonics Group, Faculty of Engineering, University of Nottingham, NG7 2RD, UK

ARTICLE INFO

Keywords:
Optical fibre sensor
Relative humidity
Absolute humidity
Temperature sensing
Layer-by-layer
Thermochromic liquid crystal

ABSTRACT

Temperature and humidity are essential parameters in monitoring the health of patients in critical care. An optical fibre sensor has been developed for simultaneous measurement of relative humidity (RH) and temperature at a single optical fibre tip based on the reflected intensity. Combining these measurements enables absolute humidity values to be obtained. The fibre tip is first modified with a coating of poly(allylamine hydrochloride) (PAH) / silica nanoparticles (SiO_2 NPs) for relative humidity (RH) measurement and then coated with thermochromic liquid crystal (TLC) for temperature measurement. Experimental results demonstrate that the RH and temperature sensitivity are respectively 0.43 %/RH% (intensity at a wavelength of 650 nm) from 55 to 90% RH ($R^2 = 0.973$) and 3.97 nm/°C from 28 to 46 °C (R^2>0.99). Moreover, the proposed sensor has low crosstalk between each of the sensing parameters, with a response time of 3.1 s temperature (30–38 °C) and 13.2 s for relative humidity (20–80 %). In comparison to grating based optical fibre sensors the proposed sensor is low-cost with a simple manufacturing process which has the potential to find widespread use in healthcare applications.

1. Introduction

Temperature and humidity are important parameters which should be controlled and adjusted in a wide range of applications, including food quality [1], human comfort [2] and clinical treatment [3]. Humidity can be divided into absolute and relative humidity: absolute humidity (AH) is the mass of water vapour in the air, relative humidity (RH) is a ratio of vapour partial pressure to the saturated vapour pressure at a given temperature [4]. In some clinical applications such as laryngectomy surgery, the upper respiratory tract is bypassed. As a result, the micro-climatic condition, especially temperature and humidity level in the nasal cavity and pharynx is changed. This can lead to some complications such as increased sputum production and chronic pulmonary disorders, all due to long term, abnormal nasal air-conditions [5]. In another example, moisture and temperature must be strictly controlled at an appropriate level during mechanical ventilation of critically ill patients, with the risk of respiratory mucosal injury, caused by drying and cooling air [6,7]. A study by Zuur *et al.* presents an approximate clinical range of moisture and temperature of air delivered to laryngectomized patients [8]. It shows that typically air (AH: 8 mg H_2O/L, 22 °C/40 % RH) is conditioned by a mechanical ventilator to 21 mg H_2O/L AH, 30 °C/70 % RH in the upper respiratory tract using a heat and moisture exchanger (HME) and 13 mg H_2O/L AH, 28 °C/50 % RH without. Monitoring temperature and humidity in real-time contributes a second safeguard for chronic patients considering the limited lifetime of an HME. In chronic wound applications, temperature and moisture are important parameters that contribute to wound healing. Armstrong *et al.* conducted a long-term skin (18-month) care study of diabetic foot ulceration of 225 subjects in which subjects were divided into two groups (standard therapy and dermal thermometry). Both groups received regular foot care and footwear, but the dermal thermometry group patients' feet were measured daily using infrared skin thermometry. This study showed that a temperature difference between feet above 4 °F (~2.2 °C) can be a trigger of early detection signs of ulceration [9]. Clinicians also recognise that wound humidity levels play an important role in healing. High humidity levels (over-wet) contribute to maceration while low humidity levels can lead to drying out of the wound [10]. Despite this, there is no definitive range of permitted humidity recommended throughout the wound healing process. Therefore, measurements and quantification of the wound microenvironment in

* Corresponding author.
E-mail address: steve.morgan@nottingham.ac.uk (S.P. Morgan).

https://doi.org/10.1016/j.snb.2021.130154
Received 3 March 2021; Received in revised form 19 May 2021; Accepted 20 May 2021
Available online 27 May 2021

terms of humidity and temperature will help in the understanding of the healing process.

Compared to electronic sensors, optical fibre sensors (OFSs) offer several advantages such as: immunity to electromagnetic interference (EMI), meaning that it can be used in electrically noisy environments such as Magnetic Resonance Imaging (MRI); small size (typical diameter of multi-mode fibre: 125 μm/62.8 μm (cladding/core)); high sensitivity; and its convenience in routing light to a remote or inaccessible location [11].

Thermochromic (TC) materials have high potential for mapping or sensing temperature. Microencapsulated ink with colour reversible thermochromism has been shown to monitor temperature [12]. A study by Kulčar et *al.* demonstrated the colorimetric properties of leuco dye thermochromic inks. These materials respond to temperature but present high hysteresis [13], attributed to the interactions with lower crystallinity between developer and solvent in the TC ink [14]. An alternative is a thermochromic liquid crystal (TLC), which is a liquid crystal with a chiral nematic phase containing a spontaneously forming macroscopic helical structure [15]. Compared with thermochromic ink, TLC exhibits negligible hysteresis in the thermally induced colour change [16] and can be utilised as a precise temperature indicator [17].

Previous research on OFSs has been proposed to measure temperature and RH based on one single fibre by using two separate fibre Bragg gratings (FBG) [18,19] or long period gratings (LPG) [20,21]. The temperature sensitivity of an FBG in the 1550 nm region is 10 pm/°C and can be used in extreme temperature conditions over the range from cryogenic (−150 °C) to high temperature (1100 °C) [22]. However, the cost of manufacturing and supporting instrumentation of gratings are relatively high, requiring a tuneable laser or high resolution spectrometer. Moreover, when the gratings are deployed in optical fibre they are affected easily by strain, which means that a temperature measurement grating must be isolated from external strain. In another non-grating temperature optical fibre sensor, Tao et al. developed an epoxy-PAH (poly(allylamine hydrochloride)) membrane coated optical fibre temperature sensor. This sensor demonstrated that the light intensity (central wavelength of 505 nm) of fluorescence emitted from the coating changed with temperature [23]. However, such optical fibre sensors based on the change in light intensity are highly dependent on stable light sources, low insertion loss connectors and are subject to bending losses.

The majority of optical fibre humidity sensors consist of a hydrophilic material such as PAH/PAA (Poly(acrylic acid)) [24,25], PVA (Poly (vinyl alcohol)) [26], titanium dioxide [27] or silicon dioxide nanospheres [28,29]. These hydrophilic materials undergo a refractive index change due to the water molecular absorption which then causes an optical signal change in the reflectivity spectrum.

Our main research interests for application of this sensor are in delivery of air to mechanically ventilated patients [21,29] and wound care for people suffering from diabetic foot ulcers [30]. In the mechanical ventilation cases, temperature and humidity should be conditioned to 29−30 °C/70 % RH with HME in the upper respiratory tract [8]. For wound care, temperature would be monitored at a slightly higher level (up to 40 °C) [31] than the normal core temperature (~37 °C) in case of infection while the humidity should be maintained at an appropriate level to avoid maceration or the wound drying out [10]. The desired RH for optimum wound dealing is less well defined with a requirement for the wound microenvironment to be 'moist' without the dressing becoming wet [32,33]. A more accurate characterisation of the RH wound microenvironment during healing may play a valuable role in understanding wound healing. In this paper, a novel hybrid sensor for simultaneously monitoring the RH and temperature at the tip of a single optical fibre has been investigated with the aim of satisfying these clinical requirements. The sensor was fabricated by firstly coating a humidity sensitive film (PAH/SiO_2) on the tip of a multi-mode optical fibre followed by a TLC solution for temperature measurement. The developed sensor demonstrates a temperature range of 28–46 °C and 20–90 %RH – both of which are advantageous for monitoring the RH and temperature in healthcare settings.

2. Materials and methods

2.1. Materials

Ethanol, Poly(allylamine hydrochloride) (Mw ~58,000, PAH), Potassium hydroxide (KOH) and Sodium hydroxide (NaOH) were purchased from Sigma-Aldrich, UK. Silica Nanoparticles (SiO_2 NPs, diameter 40–50 nm) were purchased from Nissan Chemical, Japan. Thermochromic liquid crystal (TLC, R25C5W) was supplied by LCR Hallcrest, UK. Deionised water (DI water), having resistivity of 18.2 MΩ cm, was obtained from a water purification system (PURELAB Option S/R, ELGA). Optical fibre (multimode, pigtail easy-strip 62.5/125 μm ST, A1082) was purchased from All4fiber.

2.2. Sensing mechanism

For the humidity sensing, a porous coating containing silica nanoparticles contributes to adsorb water molecules through chemisorption and physisorption [27]. The mechanism of water molecules adsorption based on SiO_2 is shown in Fig. 1. Firstly, the silica surface facilitates the dissociation of H_2O into a hydroxyl group, which binds to the silicon cation site, and a proton, which binds to an adjacent oxygen anion site. Secondly, the remaining water vapour is physisorbed with the surface hydroxyl groups through H-bonds (hydrogen-bonds). Once the first physisorbed layer is formed, the following layers are absorbed through the H-bonds. Finally, water starts to be absorbed into the pores of the coating film [27]. In addition, a poly(allylamine hydrochloride) (PAH) layer in the coating film contributes to the absorption of water molecules due to its hydrophilic property [34]. Once the sensing film is coated on the tip of the optical fibre, different levels of atmospheric humidity lead to a change of refractive index of the optical fibre tip with PAH/SiO_2 film [35].

For temperature measurements a TLC material was coated at the tip of the optical fibre. TLC molecules prefer to align parallel to each other due to the strong intermolecular attraction (π – π interactions) [36]. In the chiral nematic phase, as shown in Fig. 2, the "molecule director" spirals about a helical axis (optical axis) which is perpendicular to every molecule, and the optical properties are symmetric about this axis [15].

The resultant helical arrangement of TLC molecules has the ability to selectively reflect light of specific wavelengths (λ_s) [37] satisfying:

$$\lambda_s = \overline{n} \times p \times \cos\theta \quad (1)$$

$$\overline{n} = (n_o + n_e)/2 \quad (2)$$

Where θ is the incidence angle of the light, p is the helical pitch of the TLC which is defined as the distance it takes the molecule director to rotate 360° in the helix as illustrated in Fig. 2, n_o and n_e are the ordinary and extraordinary refractive indices, respectively. Thermal energy increases the molecule temperature of the TLC [38]: the director angle changes more rapidly, the pitch becomes shorter, causing the wavelength of the selective reflection peak to shift to the blue region. Vice versa, the wavelength shifts are longer with a temperature decrease [15]. Once the two functional films are combined in the single optical fibre tip, relative humidity and temperature will be interpreted as the total intensity change and wavelength shift of the selected peak in the reflection spectrum, respectively. The detailed signal variations are described in Sections 3.3 and 3.4.

2.3. Sensing probe fabrication

The RH sensing film (PAH/SiO_2) was coated on the multimode optical fibre tip using the layer-by-layer technique [39]. The coating step is

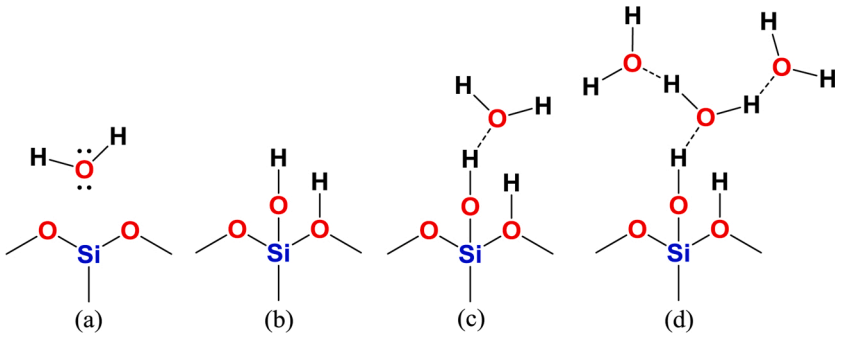

Fig. 1. Water vapour adsorption on the silica nanoparticle surface: (a) H_2O molecule close to SiO_2 surface; (b) H_2O dissociation into a -OH group binds to silicon cation site and a hydrogen proton binds to oxygen anion site; (c) and (d) the rest of H_2O were physisorbed through the hydrogen-bonds (modified from [27]).

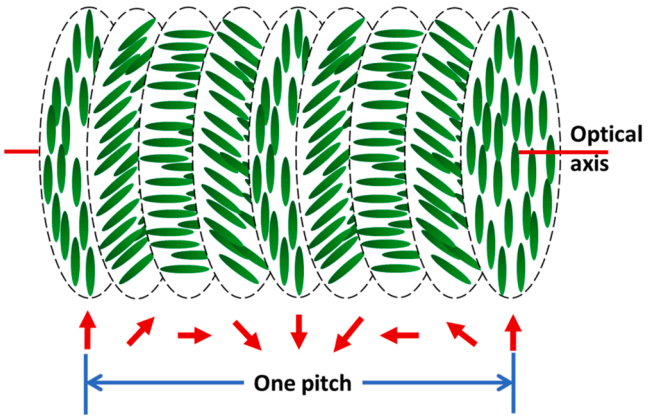

Fig. 2. The helical arrangement of molecules in the chiral nematic phase of a liquid crystal.

as follows: (i) KOH solution (Ethanol : Di-water (deionized water) = 3:2) treatment for 30 min to obtain a hydroxylated surface; (ii) after washing and drying, immerse the fibre into the positively charged PAH solution (0.17 wt%, pH = 11) for 12 min; (iii) wash and dry, and immerse the fibre in the negatively charged SiO_2 NPs solution for 12 min; (iv) repeat (ii) and (iii) steps to obtain multilayers of PAH/SiO_2 film. In order to obtain a uniform film surface, a custom made coating machine has been assembled by two stepper motors with X and Z direction stages (STANDA, 8MT175-50, Italy), as shown in Fig. 3. Subsequently, the temperature sensing film was coated with a TLC by using a dip coating machine (HO-TH-02, HOLMARC, India). After the coating process, the fibre was placed into an oven at 60 °C for 1 h for annealing. Fabrication of the different layers is conducted in this order as the hydroxylation process needed before coating PAH/SiO_2 film will damage the micro-capsule structure of the TLC material.

2.4. Experiment set-up

A climatic chamber (CVMS Climatic, Benchtop C-TH40, UK) which can set the RH in the range from 20 %RH to 98 %RH (±2.5 %RH) and temperature from −20 °C to 180 °C (fluctuation: ±0.5 °C) was used in the experiments. A type K thermocouple with data logger (Pico technology, USB TC-08 thermocouple data logger, UK) and a commercial capacitive humidity sensor (SparkFun BME280, Bosch, GER, RH range: 0%RH - 100 %RH, accuracy ±3%RH in the temperature range of -40 °C to 85 °C) were placed inside the chamber for temperature and humidity calibration. Light from a halogen source (HL-2000, Ocean Optics, UK) is coupled into a 2 × 1 fibre coupler (Newport, F-CPL-M12855, UK). The reflected light from the tip of fibre is measured by a spectrometer (USB2000+, Ocean Optics, UK) with a sampling frequency of 1 Hz.

2.5. Characterization of the OFS

The morphology of the PAH/SiO_2 film was studied using scanning electron microscopy (JEOL, JSM-7100 F, UK).

Response and recovery time of the OFS were investigated by using the set-up in Fig. 4. Firstly, the climatic chamber was set at a constant temperature and humidity level. Then the prepared OFS and commercial sensor are inserted into the chamber until both signals stabilize. Finally, the sensors are withdrawn into ambient conditions to observe how rapidly the signal recovers to a stable level. The response and recovery

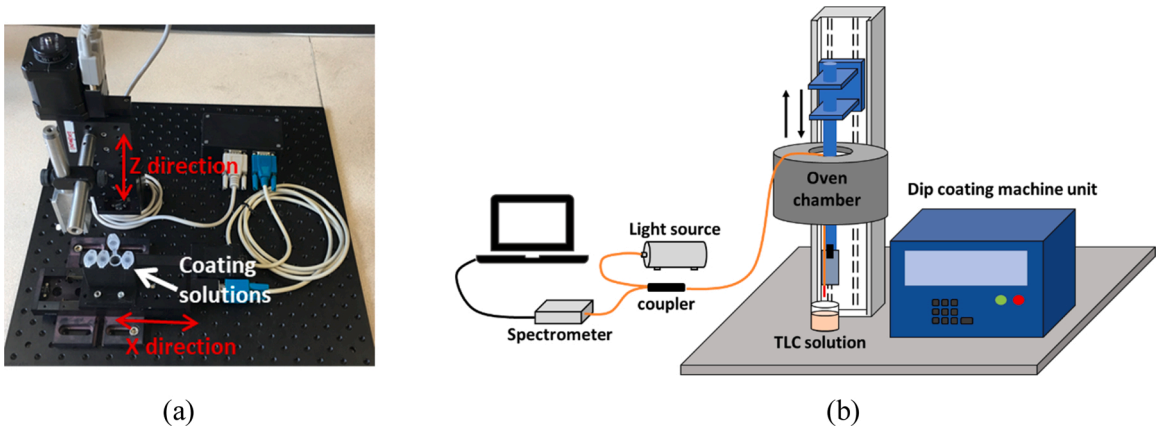

Fig. 3. (a) Custom made coating machine for layer-by-layer self-assembly which has two stepper motors (STANDA, 8MT175-50, Italy). (b) Dip coating set-up, the dip coating machine (HO-TH-02, HOLMARC, India) with an in-built oven chamber was used, the reflection spectrum was monitored by a spectrometer (USB2000, Ocean Optics, UK).

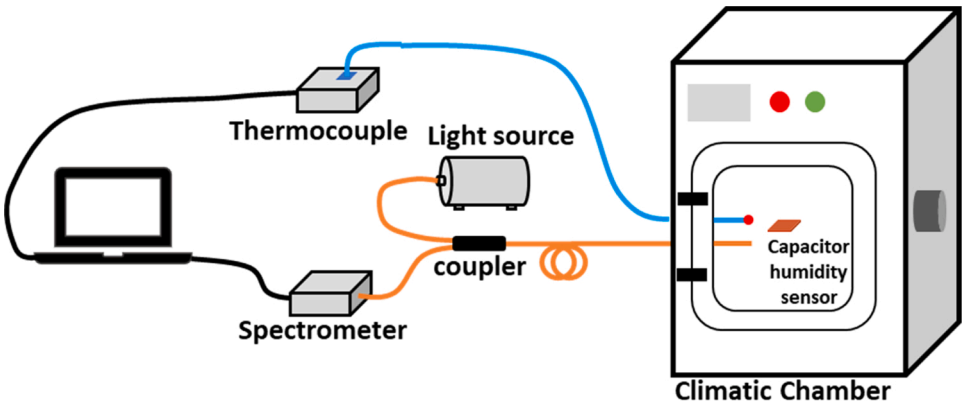

Fig. 4. Experimental set-up for the calibration, humidity and temperature measurement of OFS; a commercial capacitive humidity sensor (BME280) and a thermocouple (Pico technology, USB TC-08, UK) were placed inside the climatic chamber, the spectrometer (USB2000, Ocean Optics, UK) is connected to a PC to monitor the reflectance spectrum.

times are measured as the time between 10 %–90 % of signal change.

For humidity calibration, the RH was changed from 90 %RH to 55 % RH and reversed every 15 min with three cycles at a constant temperature of 32 °C. The reflection spectra of OFS and RH readings of the commercial humidity sensor were recorded simultaneously with the same frequency (1 Hz).

For temperature calibration, the chamber temperature is increased gradually from 28 °C to 46 °C and back, while the relative humidity was set at a constant 55 %. In order to investigate the reliability of the OFS for temperature, the OFS has been recalibrated after 20 days using the same process. The reflection spectra of the OFS and temperature reading of the thermocouple were recorded simultaneously with the same frequency (1 Hz).

For assessment of the OFS repeatability to temperature, the latter was increased from 30 °C to 37 °C (common temperature range of human body) and reversed back to 30 °C with 10 cycles while relative humidity was set at a constant 55 %.

Finally, in order to investigate the OFS performance under the changing of both temperature and humidity simultaneously, the environmental chamber temperature and humidity was set to ramp up and down three times (30 °C & 55 %RH to 37 °C & 90 %RH, respectively). The reflection spectra, temperature and humidity readings from the commercial logger were recorded simultaneously. The absolute humidity (AH) with units of mg H_2O/L can be calculated from these two parameters [40]:

$$AH = \frac{M_{H_2O} * RH * P_{ws}}{R * T};\ P_{ws}(T) = 6.112 * e^{\frac{17.67*T}{243.5+T}} \quad (4)$$

where M_{H2O} is molar mass of H_2O (18.02 g/mol), R is the gas constant which is 8.314 J/mol*K, RH and T are relative humidity and temperature value in units of % and K, respectively, $P_{ws}(T)$ is the saturation vapor pressure as a function of temperature [40]. These values are then substituted into Eq. (4) to obtain the Absolute Humidity (AH):

$$AH = \frac{2.1674 * RH * 6.112 * e^{\frac{17.67*T}{243.5+T}}}{273.15 + T} \quad (5)$$

3. Results and discussion

3.1. Optical fibre sensor fabrication

Fig. 4(a) and (b) show the SEM image of the PAH/SiO_2 only and with TLC film, respectively. It can be seen that the PAH/SiO_2 film presents a uniform morphology. The total thickness of functional film is ~750 nm which consists ~509 nm and ~243 nm for PAH/SiO_2 and TLC layers, respectively, as shown in Fig. 4(c). Fig. 4(d) shows optical images of the TLC films coated onto a glass substrate, demonstrating a gradual colour change with the temperature change. The TLC film turns from colourless to red at ~24 °C, passes through green at ~26 °C before entering blue region (28–46 °C) and, as the temperature increases above ~48 °C, turns colourless again. The sensor probe structure is shown in Fig. 4(e). The reflection spectra in Fig. 4(f) show the spectral changes before and after coating with humidity and temperature functional films. It can be seen that there has been marked drops of the whole spectrum after coating with each functional films due to the increasing refractive index of the film during the coating process based on Fresnel equation [35]. After coating with TLC, a selective reflection peak appears at 500 nm at 32 °C environmental temperature compared with the spectra before coating with TLC at the same temperature condition [41].

3.2. Response and recovery time of OFS

Fig. 5a and b show the response and recovery times of the OFS with temperature and humidity measurement, respectively, compared with a thermocouple and a commercial humidity sensor as the reference. In the temperature measurement, for OFS, the response and recovery time is calculated as 3.1 s and 57.3 s, for the thermocouple, the response and recovery time is 8.5 s and 59.1 s, respectively between 30–38 °C. In the humidity measurements, for the OFS, the response and recovery time is calculated as 13.2 s and 2.6 s whilst for the commercial humidity sensor the response and recovery time is 6.7 s and 8.9 s, respectively between 20–80 RH%. In a humid case, the interacted vapour molecule on SiO_2 film first needs to pass through the TLC film, which may cause a slightly longer response time. The optical signal recovers back once there is dissociation of water vapour with SiO_2 surface, therefore, the RH recovery time is shorter than response time.

3.3. Humidity measurement using OFS

Fig. 6(a) shows the reflection spectrum change of the OFS at a constant temperature (32 °C) with different humidity levels, 55 % and 90 %, respectively. It should be noted that there is a significant intensity change of the whole spectrum during the increase of humidity, meanwhile, the selective reflection peak of the TLC sensor remains at the same wavelength indicating the position of the peak is not affected by humidity. Fig. 6(b) illustrates the intensity change at a wavelength of 650 nm in comparison with the RH readings from the BME280 commercial humidity sensor against time. The OFS response (black trace) correlates with the change of RH (blue trace) and the reversibility to RH can be observed from the dynamic intensity change graph. In the RH calibration curve, Fig. 6(c), the response of the OFS shows a linear relationship (R^2 = 0.973) to the RH change with a sensitivity of 0.43 %/RH% (@650 nm) in the range of 55−90%. Fig. 6(d) shows the humidity cross-sensitivity evaluation of wavelength position of the

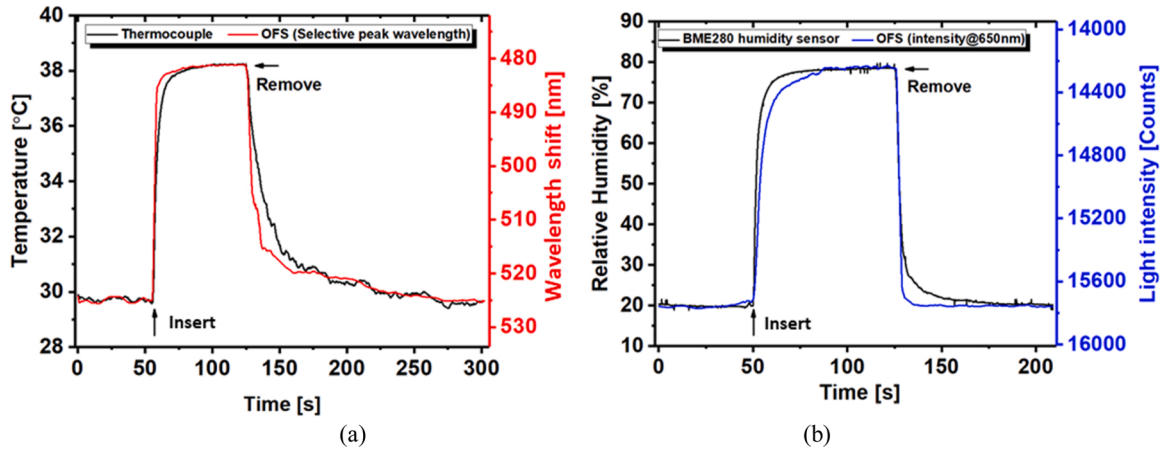

Fig. 5. (a) Response and recovery times of OFS for temperature measurement; (b) Response and recovery times of OFS for humidity measurement (BME280 – commercial humidity sensor).

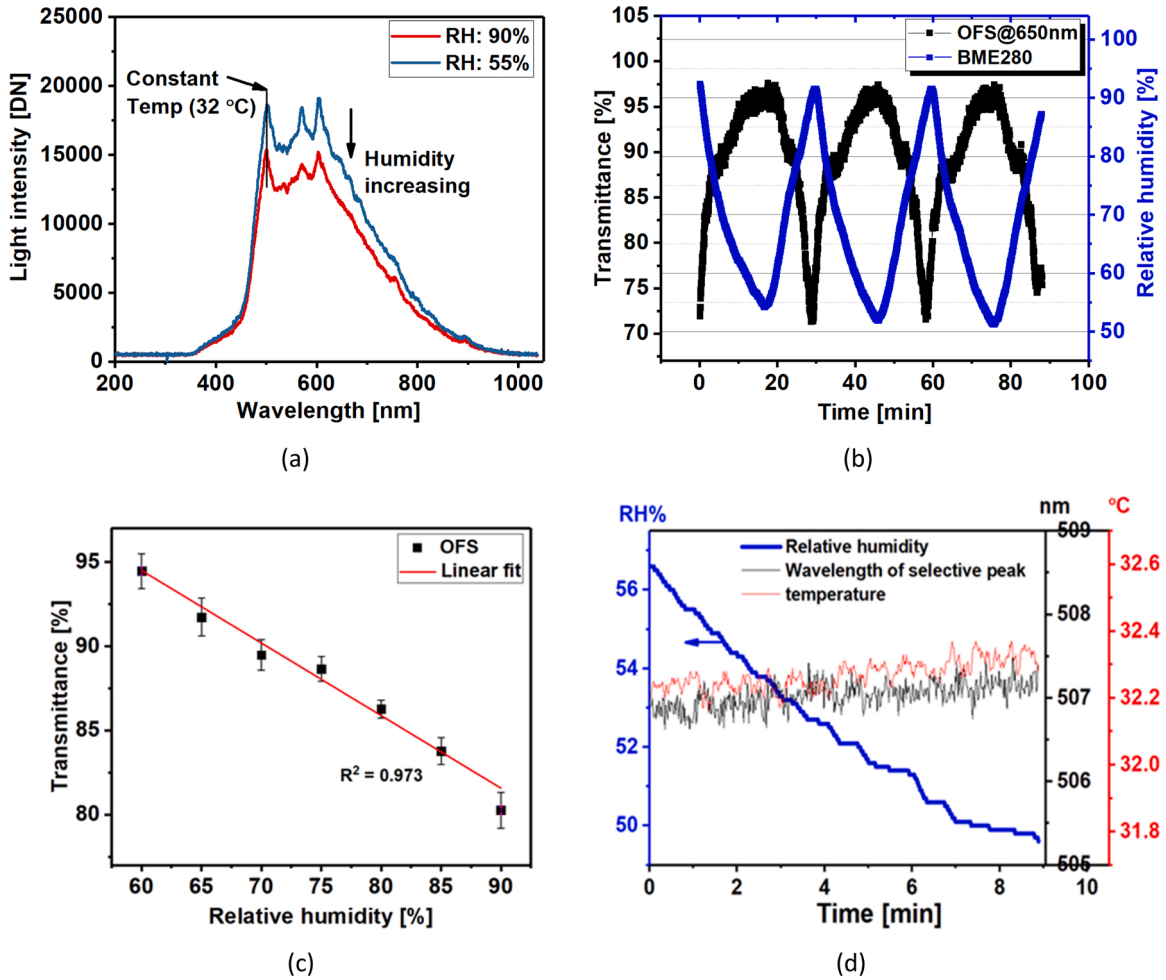

Fig. 6. (a) Reflection spectrum of OFS in 90 % RH and 55 % RH at constant temperature (32 °C). (b) The dynamic light intensity response at 650 nm wavelength of OFS in comparison to RH readings from a commercial humidity sensor. (c) The RH calibration curve of OFS (error bars represent the standard deviation of three repeat cycles). (d) Humidity crosstalk evaluation of temperature sensing film.

selective peak of the proposed hybrid sensor, the temperature was controlled at 32 °C while setting the humidity decreasing. With a 7%RH change of humidity, the wavelength of the selective peak and the temperature fluctuates at a stable level, 507 ± 0.3 nm for wavelength and 32.28 ± 0.08 °C for temperature, respectively. This relatively stable reflection value ensures the selective peak wavelength has a negligible cross-sensitivity to humidity.

OFS response (black trace) correlates with the change of RH (blue trace) and the reversibility to RH can be observed from the dynamic intensity change graph. In the RH calibration curve, Fig. 6(c), the response of the OFS shows a linear relationship ($R^2 = 0.973$) to the RH change with a sensitivity of 0.43 %/RH% (@650 nm) in the range of

55−90%.

3.4. Temperature measurement by using OFS

3.4.1. Temperature calibration

The reflection spectra of the OFS at different temperatures are shown in Fig. 7(a). No selective reflection peak exists at 22 °C, and with temperature increasing, the selective reflection peak appears and moves to the lower wavelength region. In order to investigate the reliability of the OFS, the same OFS has been recalibrated after 20 days. Fig. 7(b) represents the dynamic wavelength shift with temperature increasing and decreasing gradually between 28 °C and 46 °C on the 1 st and 20th day, respectively. This preliminary data shows robust performance. The temperature calibration curves of two test days are shown in Fig. 7(c), each point is the average of each stabilized step obtained from Fig. 7(b) and the error bar is the standard deviation of each step. The wavelength

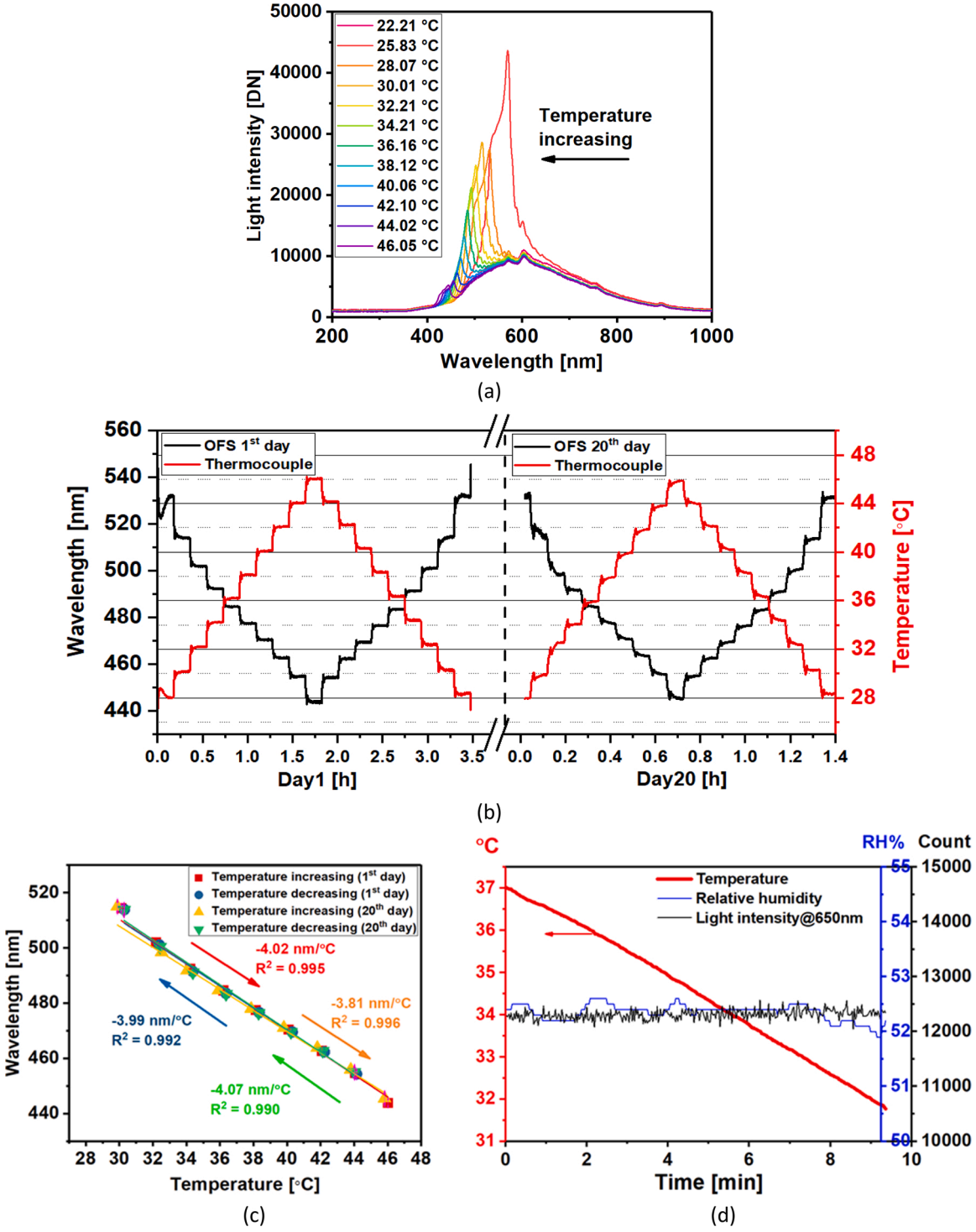

Fig. 7. (a) Reflection spectra of OFS at different temperature with the same humidity level. (b) The dynamic response of wavelength shift for selective reflection peak with changing temperature in the climatic chamber on the 1st and 20th calibration day. (c) The temperature calibration curves of OFS for 1st and 20th test day, the error bar is smaller than the marker. (d) temperature crosstalk evaluation of humidity sensing film.

shift shows linear correlation (R^2 = 0.995, 0.992, 0.996, 0.990) to the temperature which has the sensitivity of 4.02 nm/°C (temperature increasing), 3.99 nm/°C (temperature decreasing) on the first calibration day and 3.81 nm/°C (temperature increasing), 4.07 nm/°C (temperature decreasing) on the 20th calibration day, respectively. The overall temperature sensitivity obtained by taking the average of the above values is 3.97 nm/°C (STD: 0.098). It can be noticed that the linear fitting curve of each test is almost coincidental, which indicates that the OFS has a long lifetime and high accuracy for temperature sensing in the range of 28–46 °C. Fig. 7(d) illustrates the temperature cross-sensitivity evaluation for the light intensity at a wavelength of 650 nm (indicating relative humidity) of the proposed hybrid sensor, setting the temperature decreasing while the humidity remains at a relative stable level. It can be noted that the light intensity(@650 nm) and the humidity value fluctuates at a stable level when the temperature decreasing. This relatively stable reflection value ensures the light intensity(@650 nm) has a negligible cross-sensitivity to temperature.

3.4.2. *Temperature repeatability cycle test*

To further illustrate the repeatability of the prepared OFS, Fig. 8 shows the spectrum and the wavelength of the selective reflection peak change as the temperature alternates between 30 and 37 °C for 10 repeats at a constant level of humidity. The selective reflection peak moved from around 515 nm (30 °C) to 485 nm (37 °C) as shown in Fig. 8 (a). In addition, the intensity of the remaining spectrum (apart from the selective peak) remains at the same level, including the intensity at 650 nm wavelength, during the temperature measurement except for the region of the selective peak. This means the intensity change at most wavelengths is not affected by the temperature change in the range of 30−37 °C.

As shown in Fig. 8(b), the wavelength value in 30 °C and 37 °C environment tends to be a constant during the 10 thermal cycles, which indicates the performance of the OFS to temperature sensing is stable and repeatable within the tested temperature range.

3.5. *Simultaneous temperature and humidity measurement by using OFS*

To further illustrate the performance of the prepared sensor, the temperature and RH are modified simultaneously (30 °C–37 °C and 55 RH% to 90 RH%) in the climatic chamber while monitoring the spectral change of the OFS. According to the previous results, the wavelength shift of the selective reflection peak indicates the temperature change and the intensity (at 650 nm) indicates the humidity change. The dynamic change of spectra with temperature and RH increasing simultaneously is shown in Fig. 9(a), the selective peak moves left and the whole spectrum falls with temperature and RH increase, respectively. Fig. 9(b) also shows the spectrum change of the sensor in different temperature & RH environments (low: 30 °C and 55 RH%, high: 37 °C and 90 RH%).

Once the RH and temperature tests were performed, and sensitivities were obtained, the response from the sensor can be translated into a RH and temperature reading. Fig. 9(c) shows the temperature and relative humidity from the calibrated OFS during the 3 experimental tests demonstrating the results are repeatable in environments of 55 %RH & 30 °C to 90 %RH & 37 °C. The absolute humidity (AH) change, as shown in Fig. 10, was calculated from the temperature and RH values using Eq. (5). In this work, the temperature sensing is unaffected by bending or ambient light as it is a wavelength shift measurement. For the humidity sensing, the ambient light is potentially an issue in the intensity measurement cases. In this case, a fibre pigtail which contains a jacket protection along the fibre and the coating on the tip prevents ambient light being detected. In practical application, a reference bare fibre could be utilised to reduce the effects of bending losses. This has been applied in our previous work on humidity monitoring during sports [35].

The state of the art in hybrid optical fibre sensors for humidity and temperature sensing is presented in Table 1. It can be seen that our current hybrid sensor exhibits a higher sensitivity to temperature (3.97 nm/°C), although it cannot be directly compared to the RH sensitivity due to the different response units (intensity base in this work). The temperature measuring range of the proposed sensor is narrower compared with other types of sensor in the table, which is 28−46 °C, however, it is ideally suited to many healthcare applications. The cost of using an OFS based on gratings is much higher than reflection type optical fibre sensors, thus, the proposed sensor has the potential for widespread use. The use of a spectrometer reduces the cost compared to most optical fibre interrogators which brings it into the range that would be acceptable as a medical device used in critical care or wound clinics. It may be possible in future to implement the system using an array of LEDs which cover the operating wavelength range of the sensor, demonstrating a roadmap to very low cost, wearable devices. Moreover, the proposed hybrid sensor is able to measure at a single sensing point for RH and temperature, which allows sensor to operate in a confined environment, compared to other types of optical fibre sensors.

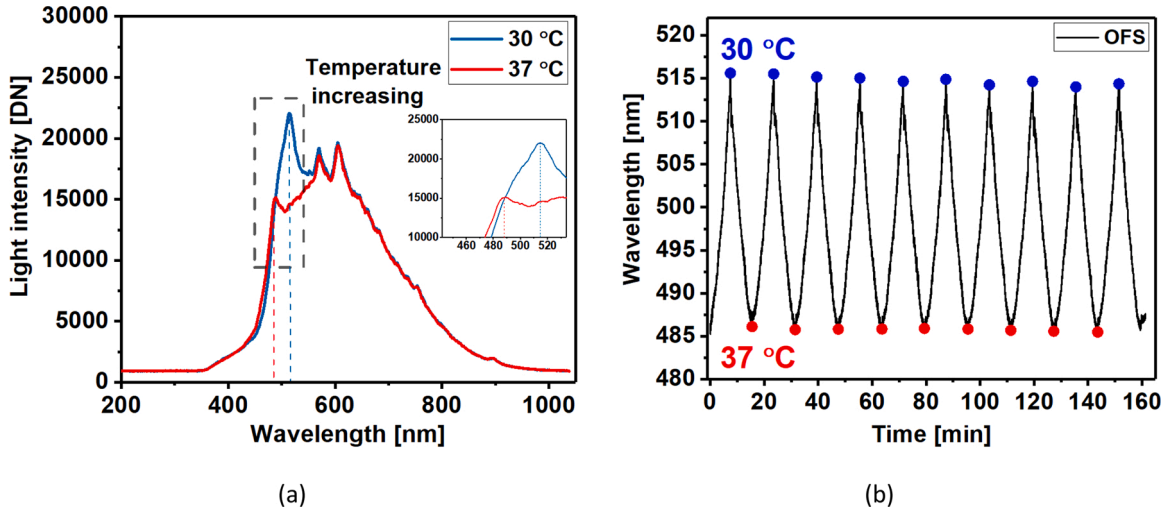

Fig. 8. (a) The reflection spectrum of OFS at different temperature (blue line for 30 °C and red line for 37 °C) at constant humidity level of 50 RH%, inset shows region around the selective peak. (b) The wavelength shift of the selective reflection peak under alternating temperature.

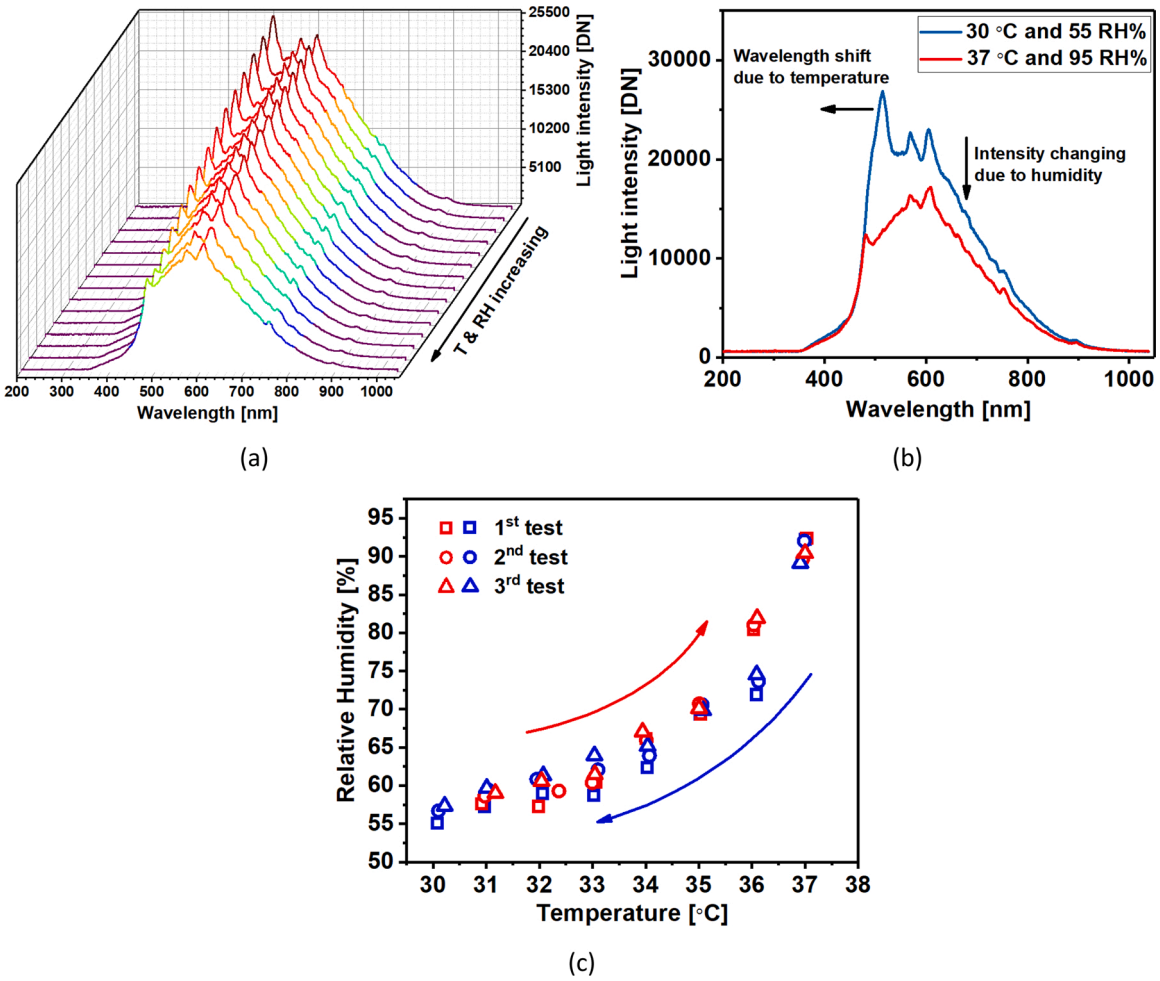

Fig. 9. (a) The spectrum changes with temperature and RH increasing simultaneously. (b) The reflection spectrum in low (blue curve) and high (red curve) temperature & RH environment, the wavelength shift and intensity change due to temperature and RH, respectively. (c) Hybrid sensor response for changing RH and temperature simultaneously, square, circle and triangle represent 1st, 2nd and 3rd test, red and blue for increasing and decreasing process respectively.

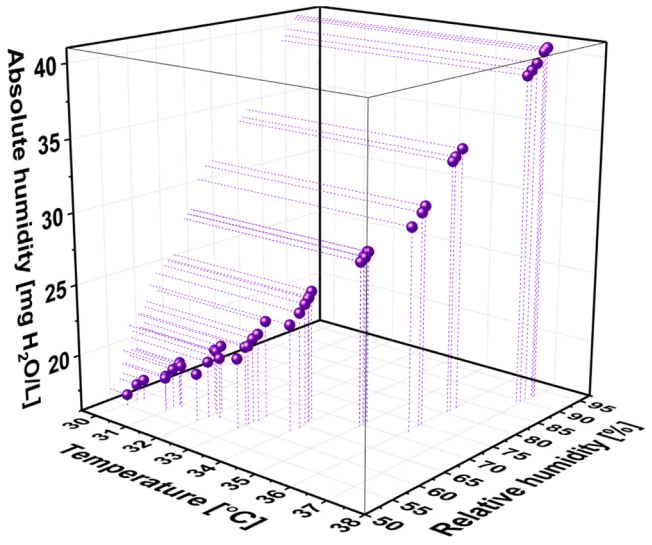

Fig. 10. Absolute humidity calculated from the simultaneous temperature and RH measurements, in the ranges of 30-37 °C and 55-90 %, respectively.

4. Conclusions

A novel optical fibre hybrid sensor for monitoring relative humidity and temperature was developed by coating the tip of a single optical fibre with PAH/SiO_2 for relative humidity, and a thermochromic liquid crystal for temperature. The reflected intensity changes in response to the refractive index change of the PAH/SiO_2 film that absorbs water molecules at different RH. The signal response to RH was linear ($R^2 = 0.973$) with a sensitivity of 0.43 %/RH% in the RH range of 55%–90%. The selective reflection peak showed the sensitivity to temperature and a linear relationship ($R^2 = 0.993$) between peak wavelength shift and temperature with a sensitivity of 3.97 nm/°C over the temperature range of 28–46 °C. In addition, the simultaneous RH and temperature measurement is repeatable over several cycles. Also, the proposed sensor has the potential for measuring absolute humidity to generate additional information in clinical applications. This simple to manufacture, low-cost and novel hybrid sensor has the potential to be used in many healthcare applications.

CRediT authorship contribution statement

Chenyang He: Conceptualisation, Methodology, Software, Validation, Formal analysis, Investigation, Writing - original draft. **Serhiy Korposh:** Conceptualisation, Methodology, Writing - review & editing, Supervision, Funding acquisition. **Ricardo Correia:** Methodology, Validation, Investigation, Writing - review & editing, Supervision,

Table 1
Comparison of different RH and temperature optical fibre sensors. '- 'indicates the information is not provided in the cited work.

Optical fibre sensor structure	RH sensitivity & range	Temperature sensitivity & range	Sensing region	Response time	Ref
Array of LPGs	0.53 nm/RH% (35−98%)	0.46 nm/°C (25−38 °C)	6cm	RH: - T: -	[21]
Functional tip & FBG	– (11−97%)	0.01 nm/°C (10−85 °C)	5 mm + fibre tip(Ø:125 μm)	RH: <1.5s T: -	[42]
Partially-coated LPG	0.063 nm/RH% (20−80%)	0.41 nm/°C (25−85 °C)	6cm	RH: - T: -	[20]
Polymer fibre FBG	0.007 nm/RH% (10−90%)	0.03 nm/°C (20−100 °C)	2mm	RH: - T: -	[43]
Suspended-core fibre	–	0.01 nm/°C (20−1100 °C)	Fibre tip (only temperature)	T: -	[44]
Hybrid functional tip	0.43 %/RH% (55−90%)	3.97 nm/°C (28−46 °C)	One fibre tip (Ø:125 μm)	RH: 13.2 s T: 3.1 s	This work

Funding acquisition. **Liangliang Liu:** Methodology, Writing - review & editing. **Barrie R. Hayes-Gill:** Validation, Writing - review & editing, Supervision, Funding acquisition. **Stephen P. Morgan:** Conceptualisation, Writing - review & editing, Supervision, Project administration, Funding acquisition.

Declaration of Competing Interest

The authors report no declarations of interest.

Acknowledgements

This work was funded by the Engineering and Physical Sciences Research Council (UK) (Grant number EP/N026985/1) and the Medical Research Council (MR/R025266/1). SPM is supported by a Royal Society Industry Fellowship. The authors would like to thank the Nanoscale and Microscale Research Centre (nmRC) at the University of Nottingham for providing access to the instrumentation, and Mike Parsley and Peter Rigby of LCR Hallcrest Ltd for TLC supply and useful discussions.

References

[1] V. Stojceska, P. Ainsworth, A. Plunkett, Ş. İbanoğlu, The effect of extrusion cooking using different water feed rates on the quality of ready-to-eat snacks made from food by-products, Food Chem. 114 (1) (2009) 226–232.
[2] A.V. Arundel, E.M. Sterling, J.H. Biggin, T.D. Sterling, Indirect health effects of relative humidity in indoor environments, Environ. Health Perspect. 65 (1986) 351–361.
[3] C.L. Lim, C. Byrne, J.K. Lee, Human thermoregulation and measurement of body temperature in exercise and clinical settings, Ann. Acad. Med. Singap. 37 (4) (2008), p. 347.
[4] M. Shelly, G. Lloyd, G. Park, A review of the mechanisms and methods of humidification of inspired gases, Intensive Care Med. 14 (1) (1988) 1–9.
[5] J.K. Zuur, S.H. Muller, A. Vincent, M. Sinaasappel, F.H. De Jongh, F.J. Hilgers, Assessment of tracheal temperature and humidity in laryngectomized individuals and the influence of a heat and moisture exchanger on tracheal climate, Head Neck 30 (8) (2008) 1072–1082.
[6] G. Thiéry, et al., Heat and moisture exchangers in mechanically ventilated intensive care unit patients: a plea for an independent assessment of their performance, Crit. Care Med. 31 (3) (2003) 699–704.
[7] N.K. Nakagawa, et al., Effects of a heat and moisture exchanger and a heated humidifier on respiratory mucus in patients undergoing mechanical ventilation, Crit. Care Med. 28 (2) (2000) 312–317.
[8] J. Zuur, S. Muller, F.H. de Jongh, N. Van Zandwijk, F. Hilgers, The physiological rationale of heat and moisture exchangers in post-laryngectomy pulmonary rehabilitation: a review, Eur. Arch. Otorhinolaryngol. 263 (1) (2006) 1–8.
[9] D.G. Armstrong, K. Holtz-Neiderer, C. Wendel, M.J. Mohler, H.R. Kimbriel, L. A. Lavery, Skin temperature monitoring reduces the risk for diabetic foot ulceration in high-risk patients, Am. J. Med. 120 (12) (2007) 1042–1046.
[10] T.R. Dargaville, B.L. Farrugia, J.A. Broadbent, S. Pace, Z. Upton, N.H. Voelcker, Sensors and imaging for wound healing: a review, Biosens. Bioelectron. 41 (2013) 30–42.
[11] J. Ascorbe, J.M. Corres, F.J. Arregui, I.R. Matias, Recent developments in fiber optics humidity sensors, Sensors 17 (4) (2017), p. 893.
[12] O. Panák, M. Držková, M. Kaplanová, Insight into the evaluation of colour changes of leuco dye based thermochromic systems as a function of temperature, Dye. Pigment. 120 (2015) 279–287.
[13] R. Kulčar, M. Friškovec, N. Hauptman, A. Vesel, M.K. Gunde, Colorimetric properties of reversible thermochromic printing inks, Dye. Pigment. 86 (3) (2010) 271–277.
[14] M. Hajzeri, K. Bašnec, M. Bele, M.K. Gunde, Influence of developer on structural, optical and thermal properties of a benzofluoran-based thermochromic composite, Dye. Pigment. 113 (2015) 754–762.
[15] I. Sage, Thermochromic liquid crystals, Liq. Cryst. 38 (11-12) (2011) 1551–1561.
[16] C. Smith, D. Sabatino, T. Praisner, Temperature sensing with thermochromic liquid crystals, Exp. Fluids 30 (2) (2001) 190–201.
[17] C. He, S. Korposh, R. Correia, B. Hayes-Gill, S. Morgan, Optical fibre temperature sensor based on thermochromic liquid crystal, in: International Society for Optics and PhotonicsSeventh European Workshop on Optical Fibre Sensors, 11199, 2019, p. 1119908.
[18] C. Zhang, W. Zhang, D.J. Webb, G.-D. Peng, Optical fibre temperature and humidity sensor, Electron. Lett. 46 (9) (2010) 643–644.
[19] M. Ams, et al., Fibre optic temperature and humidity sensors for harsh wastewater environments, in: 2017 Eleventh International Conference on Sensing Technology (ICST), IEEE, 2017, pp. 1–3.
[20] A. Urrutia, J. Goicoechea, A.L. Ricchiuti, D. Barrera, S. Sales, F.J. Arregui, Simultaneous measurement of humidity and temperature based on a partially coated optical fiber long period grating, Sens. Actuators B Chem. 227 (2016) 135–141.
[21] J. Hromadka, et al., Simultaneous in situ temperature and relative humidity monitoring in mechanical ventilators using an array of functionalised optical fibre long period grating sensors, Sens. Actuators B Chem. 286 (2019) 306–314.
[22] B. Zhang, M. Kahrizi, High-temperature resistance fiber Bragg grating temperature sensor fabrication, IEEE Sens. J. 7 (4) (2007) 586–591.
[23] S. Tao, A. Jayaprakash, A fiber optic temperature sensor with an epoxy-glue membrane as a temperature indicator, Sens. Actuators B Chem. 119 (2) (2006) 615–620.
[24] D. Lopez-Torres, et al., Photonic crystal fiber interferometer coated with a PAH/PAA nanolayer as humidity sensor, Sens. Actuators B Chem. 242 (2017) 1065–1072.
[25] I. Del Villar, I.R. Matías, F.J. Arregui, R.O. Claus, Fiber-optic hydrogen peroxide nanosensor, IEEE Sens. J. 5 (3) (2005) 365–371.
[26] T. Li, X. Dong, C.C. Chan, K. Ni, S. Zhang, P.P. Shum, Humidity sensor with a PVA-coated photonic crystal fiber interferometer, IEEE Sens. J. 13 (6) (2013) 2214–2216.
[27] C. Huang, et al., Optical fiber humidity sensor with porous TiO 2/SiO 2/TiO 2 coatings on fiber tip, Ieee Photonics Technol. Lett. 27 (14) (2015) 1495–1498.
[28] J.M. Corres, I.R. Matias, M. Hernaez, J. Bravo, F.J. Arregui, Optical fiber humidity sensors using nanostructured coatings of SiO $ _ {2} $ nanoparticles, IEEE Sens. J. 8 (3) (2008) 281–285.
[29] F.U. Hernandez, et al., Characterization and use of a fiber optic sensor based on PAH/SiO 2 film for humidity sensing in ventilator care equipment, IEEE Trans. Biomed. Eng. 63 (9) (2016) 1985–1992.
[30] D. Gomez, S.P. Morgan, B.R. Hayes-Gill, R.G. Correia, S. Korposh, Polymeric optical fibre sensor coated by SiO2 nanoparticles for humidity sensing in the skin microenvironment, Sens. Actuators B Chem. 254 (2018) 887–895.
[31] D. Lou, et al., Flexible wound healing system for pro-regeneration, temperature monitoring and infection early warning, Biosens. Bioelectron. 162 (2020), p. 112275.
[32] S.D. Milne, et al., A wearable wound moisture sensor as an indicator for wound dressing change: an observational study of wound moisture and status, Int. Wound J. 13 (6) (2016) 1309–1314.
[33] C.R. Kruse, et al., The external microenvironment of healing skin wounds, Wound Repair Regen. 23 (4) (2015) 456–464.
[34] A. Schulze, et al., Permanent surface modification by electron-beam-induced grafting of hydrophilic polymers to PVDF membranes, RSC Adv. 3 (44) (2013) 22518–22526.
[35] C. He, et al., Real-time humidity measurement during sports activity using optical fibre sensing, Sensors 20 (7) (2020), p. 1904.
[36] J.-G. An, S. Hina, Y. Yang, M. Xue, Y. Liu, Characterization of liquid crystals: a literature review, Rev. Adv. Mater. Sci. 44 (4) (2016).
[37] R. Alben, Theory of the change in cholesteric pitch near cholesteric-smectic phase transitions, Mol. Cryst. Liq. Cryst. 20 (3-4) (1973) 231–238.

[38] P.P. Gaikwad, M.T. Desai, Liquid crystalline phase and its Pharma application, Int. J. Pharma Res. Rev. 2 (12) (2013) 40–52.
[39] S. Korposh, T. Wang, S. James, R. Tatam, S.-W. Lee, Pronounced aromatic carboxylic acid detection using a layer-by-layer mesoporous coating on optical fibre long period grating, Sens. Actuators B Chem. 173 (2012) 300–309.
[40] D. Bolton, The computation of equivalent potential temperature, Mon. Weather. Rev. 108 (7) (1980) 1046–1053.
[41] L. Van Der Werff, et al., Thermochromic composite fibres containing liquid crystals formed via melt extrusion, J. Mater. Sci. 48 (14) (2013) 5005–5011.
[42] F.J. Arregui, I.R. Matías, K.L. Cooper, R.O. Claus, Simultaneous measurement of humidity and temperature by combining a reflective intensity-based optical fiber sensor and a fiber Bragg grating, IEEE Sens. J. 2 (5) (2002) 482–487.
[43] G. Woyessa, A. Fasano, C. Markos, H.K. Rasmussen, O. Bang, Low loss polycarbonate polymer optical fiber for high temperature FBG humidity sensing, IEEE Photonics Technol. Lett. 29 (7) (2017) 575–578.
[44] L.V. Nguyen, S.C. Warren-Smith, H. Ebendorff-Heidepriem, T.M. Monro, Interferometric high temperature sensor using suspended-core optical fibers, Opt. Express 24 (8) (2016) 8967–8977. Apr 18.

Chenyang He is a Research Fellow in the Optics and Photonics Research Group, University of Nottingham, for developing a smart endotracheal tube that can monitor the microcirculation in trachea from Dec. 2020. He will be awarded the PhD degree at Faculty of Engineering, University of Nottingham on Aug. 2021. The main research interests include designing and fabrication of new type of optical fibre sensing system and further investigation for healthcare applications. During his PhD study, he contributed to 9 scientific works (6 peer review journal articles, 3 conference proceeding papers).

Dr Serhiy Korposh received both his bachelor and master degrees in 2001 and 2002 respectively in physics from Uzhgorod National University, Transcarpathia (Ukraine) and Ph.D. degree from Cranfield University in 2007. He worked as a post-doctoral researcher on development of the novel materials for chemical sensors in the Graduate School of Environmental Engineering of the University of Kitakyushu from 2008 to 2012. From 2012–2013 he worked as a research fellow in the Department of Engineering Photonics, Cranfield University. Since 2013 he is an Associate Professor at the University of Nottingham. His research interest lies in the field of development of fibre-optic chemical sensors modified with the sensitive materials and their applications in healthcare and environmental monitoring.

Ricardo Goncalves Correia is an assistant Professor in Optical Fibre Sensing at the University of Nottingham. As an Instrumentation Engineer specialised in the development of fibre optic sensors, his research passion focusses on the development and application of fibre optic sensors for a wide range of applications that range from healthcare to civil engineering and aerospace. His main interest is in the development and application of fibre optic sensors for physical measurements.

LiangLiang Liu is a research fellow working in the Optics and Photonics Group, University of Nottingham, UK. His research interest is to develop implantable photonics sensing devices for disease monitoring and interaction of neural activities

Barrie Hayes-Gill is Professor of Medical Devices and Electronic Systems at the University of Nottingham. His research covers a broad range of the application of electronic engineering and optical systems to medical devices with an emphasis on technology transfer. Some of his recent work has involved the deployment of an optical sensor in a newborn's cap to monitor heart rate and oxygen saturation at birth along with the deployment of fibre optic sensors in wearable medical devices in both hospital and home settings. Most significantly he has developed a wearable fetal monitor for mothers at birth which is now being deployed in thousands of births around the world. He is a Chartered Engineer and Fellow of the Institution of Engineering Technology.

Stephen Morgan is Professor of Biomedical Engineering at the University of Nottingham. His research involves the development of devices to monitor the microcirculation specifically in tissue breakdown and wound healing. For example, he currently developing a novel endotracheal tube that can monitor the microcirculation at the cuff/trachea interface. Recent work involves the development of photonic textiles. These sensing systems, incorporated into garments can monitor pressure, temperature, the microcirculation and other biomarkers. His work has involved close collaboration with numerous industry partners. He is a Royal Society Industry Fellow and Academic Director of the Centre for Healthcare Technologies which aims to bring together key stakeholders, capabilities and expertise to support the rapid translation of scientific discoveries into healthcare adoption.